Korean J. Chem. Eng., 37(12), 2368-2383 (2020)
DOI: 10.1007/s11814-020-0660-9

pISSN: 0256-1115
eISSN: 1975-7220

Influence of frictional packing limit on hydrodynamics and performance of gas-solid fluidized beds

Akhilesh Kumar Sahu†, Vasudevan Raghavan, and Bhamidi Prasad

Department of Mechanical Engineering, Indian Institute of Technology Madras Chennai 600036, India
(*Received 1 April 2020 • Revised 12 August 2020 • Accepted 17 August 2020*)

Abstract−The influence of frictional packing limit (*FPL*) on prediction of hydrodynamics and performance of fluidized bed reactors was studied. Dense gas-solid flows in non-reactive (under isothermal cold and at elevated temperatures) and reactive atmospheres (fluidized bed gasifier) were simulated using Eulerian-Eulerian methodology considering a range of values for *FPL*. Simulations under cold flow conditions were conducted to establish a range of *FPL* values that provides physically realistic predictions. It is noticed that bed pressure drop increases with increasing value of *FPL* when superficial gas velocity (*U*) is less than or equal to the minimum fluidization velocity. For larger values of *U*, predicted pressure drop is unaffected by the choice of value of *FPL*. However, in these cases, the distribution of particles, their velocities and bubbling behavior are significantly affected by *FPL*. Effect of *FPL* at elevated temperatures is similar to the one observed at cold flow conditions. It is further noticed that *FPL* not only affects the predictions on bed hydrodynamics but also has profound influence on reactive flow characteristics such as bed temperature and product gas composition. Sensitivity analysis under cold flow conditions could reveal better predictions when the ratio of *FPL* to close packing limit is chosen between 0.9 and 0.97.

Keywords: Frictional Packing Limit, Hydrodynamics, Fluidized Bed Reactors, Dense Gas-solid Flows, Minimum Fluidization Velocity

INTRODUCTION

Factors such as excellent mixing, enhanced heat and mass transfer characteristics and better control over emissions resulted in the use of fluidized bed reactors in the power sector. These reactors often operate in dense solid-gas regime such as bubbling beds. Despite being discovered almost a century ago, understanding of hydrodynamics of gas-solid flows in these reactors is still evolving. Experimental studies have been carried out on lab/pilot scale cold flow reactors to facilitate flow visualization. While choking of the probe by particles is a problem, bed pressure drop and static pressure have been measured reasonably well. However, experimental determination of other hydrodynamic parameters such as velocity of gas and particles, solid mass flux, particle mixing and bubble characteristics are quite involved even under cold flow conditions and more complexity arises in reactive ambience. Therefore, numerical simulation is often used to assist in scale up design of fluidized bed reactors. There are two approaches to simulate particle laden flows: Eulerian-Lagrangian (E-L) methodology and kinetic theory of granular flow (KTGF) based Eulerian-Eulerian (E-E) approach.

E-L methodology based gas-solid flow simulations, employing different variants such as discrete particle model [1], computational fluid dynamics-discrete element method [2] are reported in literature besides direct numerical simulation based studies [3]. However, at present, as reviewed elsewhere [4], E-E methodology is more favorable for modeling particle laden flows in fluidized beds. E-E approach considers fluid as well as particles as interpenetrating continua. Flow dynamics is simulated by solving-continuum equations obtained using ensemble averaging method as discussed in Musser and Carney [5]. Solution of these equations requires closure for terms associated with inter-phase exchange and solids phase stresses. Constitutive correlations to close solids phase stress terms are derived using kinetic theory of granular flow (KTGF) assuming particle-particle collision binary and instantaneous, analogous to application of the theory to dense gases. However, frictional forces arising due to enduring contacts among particles are ignored in KTGF based approach. To account for particle-particle frictional stresses, models are proposed in literature based on theory of soil mechanics. Considering granular material as visco-plastic fluid Jop et al. [6] suggested constitutive law to account for particle-particle frictional effects in dense gas-solid flows. In their method, frictional stress is estimated in terms of normal component of stress, and a proportionality constant that depends on shear rate, particle size, particle density and dimensionless friction parameters. Farzaneh et al. [7] compared bed hydrodynamics predicted using frictional stress models reported in Schaeffer [8], Srivastava and Sundaresan [9] and Jop et al. [6]. They found better predictions for particle velocity, gas-solid flow pattern and horizontal dispersion coefficient when Jop et al. [6] model was used.

Johnson and Jackson [10] and Johnson et al. [11] reported correlations to determine frictional pressure (normal component of frictional stress) in terms of material properties, solids volume fraction, frictional packing limit and close packing limit. Frictional packing limit is the threshold value of solid volume fraction at which frictional stresses become significant and are included in the model. Close packing limit is the maximum attainable value of particle vol-

†To whom correspondence should be addressed.
E-mail: aksahu.iitm@gmail.com

ume fraction in a fluidized bed. Further, frictional viscosity is estimated as a function of normal component of stress, angle of internal friction and second invariant of deviatoric strain rate tensor. The extent of cohesiveness of powder is accounted by the angle of internal friction and its value varies between 15° and 45° [12] depending on material properties. Schaeffer [8] reported a correlation to estimate frictional viscosity, which several investigators have employed [13-17]. Syamlal et al. [13] suggested an empirical correlation to determine frictional pressure accounting for viscous as well as plastic regime. Srivastava and Sundaresan [9] employed a combination of frictional pressure models reported by Johnson et al. [11] and Syamlal et al. [13] besides including an additional term accounting for the fluctuations in strain rate tensor.

Shuyan et al. [18] investigated the hydrodynamics of gas-solid flows in a spouted bed by incorporating the effects of particle-particle friction in KTGF based model. Combination of Johnson and Jackson [10] model for frictional pressure and Schaeffer [8] model for frictional viscosity was used. With a close packing limit (*CPL*) of 0.593, gas-solid flow dynamics was examined for frictional packing limit (*FPL*) values of 0.4, 0.45 and 0.5. They noted an increase granular temperature and gas volume fraction with increasing value of *FPL* in the spout region and a reversed trend in the annulus region. Passalacqua and Marmo [19] compared bubble characteristics of a central jet as well as uniformly fluidized beds obtained using various models for frictional pressure. Sensitivity of frictional packing limit towards prediction of bubble size was examined by employing *FPL* values of 0.5 and 0.63 within the frictional stress model of Srivastava and Sundaresan [9] for *CPL*=0.65. Bubble size was under-predicted with *FPL* value of 0.5, whereas a better match with experimental data was noted with *FPL*=0.63. Hosseini et al. [20] compared particle velocities obtained using *FPL* values of 0.5 and 0.6 in a spouted bed using Srivastava and Sundaresan [9] model. Under-prediction of particle velocity in the spout zone was observed for *FPL* value of 0.5. Rahimi et al. [21] reported influence of *FPL* on hydrodynamics of gas-solid flows in a two-dimensional vibrating fluidized bed using a modified form of Srivastava and Sundaresan [9] frictional stress model. Four *FPL* values ranging from 0.45 to 0.6 were employed. They found an increase in predicted pressure drop, expanded bed height and particle velocity with increasing value of *FPL*. Unlike Passalacqua and Marmo [19], better predictions were claimed with the smallest examined *FPL* value of 0.45. Sahu et al. [22] emphasized the importance of selecting appropriate sub-model for frictional pressure and a suitable value of *FPL* to simulate dense gas-solid flows under isothermal cold flow conditions for a specified value of *CPL* However, a range of *FPL* value giving realistic predictions of dense gas-solid flows was not reported.

As evident from literature, only few investigators have reported the effects of *FPL* on hydrodynamics of dense gas-solid flows under cold flow conditions for a particular value of *CPL*. However, studies quantifying the influence of *FPL* for different values of *CPL* are scarce. Moreover, effects of *FPL* on hydrodynamics and performance of a fluidized bed reactor operating at elevated temperatures and in a reactive environment remain unexplored. Therefore, the present study aimed to examine the sensitivity of *FPL* towards the prediction of hydrodynamics and performance of a bubbling fluidized bed gasifier (operating in a reactive ambience) besides suggesting a range of *FPL* values giving realistic predictions in terms of *CPL* under cold flow conditions. Combination of frictional pressure model (*FPM*) of Johnson et al. [11] and frictional viscosity model of Schaeffer [8] was employed to study the sensitivity of frictional packing limit.

COMPUTATIONAL MODEL, SOLUTION METHODOLOGY AND MODEL VALIDATION

Eulerian-Eulerian multi-phase flow methodology available in ANSYS FLUENT 15.0 was implemented. Equations governing the transport phenomena along with constitutive correlations and different sub-models under isothermal cold flow, non-reactive hot flow and reactive flow inside fluidized bed coal gasifier have been extensively reported elsewhere [4, 22 and 23]. User defined functions have been used to implement the rates of heterogeneous reactions such as moisture release, volatile cracking, tar cracking, char oxidation, steam gasification, CO_2 gasification, methanation and tar oxidation. For the sake of brevity, only constitutive correlations pertaining to solids phase stress tensor and equations to estimate gas-solid interphase exchange coefficient, bed pressure drop and minimum fluidization velocity are provided in the following sub-section.

1. Solids Phase Stresses

Brief description of momentum balance equation and constitutive correlations to evaluate various terms associated with solids stresses is presented subsequently.

Particle phase momentum balance equation:

$$\frac{\partial(\alpha_s\rho_s\bar{v}_s)}{\partial t}+\nabla\cdot(\alpha_s\rho_s\bar{v}_s\bar{v}_s)=-\alpha_s\nabla p_s+\nabla\cdot\bar{\bar{\tau}}_s+\alpha_s\rho_s\bar{g}+K_{sg}(\bar{v}_g-\bar{v}_s)+\bar{v}_sS_s \quad (1)$$

Expression reported by Lun et al. [24] is used to determine solids pressure (p_s). Solids pressure term is used to avoid unphysical compaction of particles [18].

$$p_s=\alpha_s\rho_s\theta_s+2\rho_s\alpha_s^2g_0\theta_s(1+e_{ss}) \quad (2)$$

Solids stress tensor is estimated using the following expression:

$$\bar{\bar{\tau}}_s=\alpha_s\mu_s(\nabla\bar{v}_s+\nabla\bar{v}_s^T)+\alpha_s(\lambda_s-(2/3)\mu_s)\nabla\cdot\bar{v}_s\bar{\bar{I}} \quad (3)$$

Here λ_s is the bulk viscosity of solids phase and is calculated using the correlation suggested by Lun et al. [24].

$$\lambda_s=\frac{4}{3}\alpha_s\rho_sd_sg_0(1+e_{ss})\sqrt{\frac{\theta_s}{\pi}} \quad (4)$$

In dense gas-solid flows frictional component of viscosity is also included in addition to kinetic and collisional components. Thus, solids viscosity is written as linear combination of kinetic (translational), collisional and frictional contributions.

$$\mu_s=\mu_{s,kin}+\mu_{s,col}+\mu_{s,fr} \quad (5)$$

$$\mu_{s,kin}=\frac{\alpha_s\rho_sd_s\sqrt{\theta_s\pi}}{6(3-e_{ss})}+\left\{1+\frac{2}{5}\alpha_sg_0(1+e_{ss})(3e_{ss}-1)\right\} \quad (6)$$

$$\mu_{s,col}=\frac{4}{5}\alpha_s^2\rho_sd_sg_0(1+e_{ss})\sqrt{\frac{\theta_s}{\pi}} \quad (7)$$

Table 1. Column dimensions, particle properties and model parameters used to simulate cold (T=303 K) and non-reactive hot (T=473 K) flow cases

Parameter	Escudero [27] (Cold flow)	England [28] (Cold flow)	Jiliang et al. [29] (Hot flow)
Column diameter (mm)	102	76.2	80
Column height (mm)	910	254	650
Particle density (kg/m^3)	2,600	2,000	2,750
Particle size (mm)	0.55	0.348	0.5
Computational domain	3D	3D	3D
Number of cells	69,160	10,863	90,816
Static bed height (mm)	204	64.5	144.5
Initial solid volume fraction	0.59	0.62	0.6
Close packing limit	0.63 and 0.65	0.65	0.65
Frictional packing limit	0.5, 0.55, 0.58 0.61 and 0.63		0.5, 0.55, 0.61, 0.63
Coefficient of restitution	0.9	0.9	0.9
Specularity coefficient	0.05	0.05	0.05
Time step size (s)	0.00025	0.00025	0.00025
Max. iterations/time step	50	50	50
Simulation time (s)	20	20	20

$$\mu_{s,fr}=\frac{p_{fr}\sin\emptyset}{2\sqrt{I_{2D}}} \tag{8}$$

Here, $\mu_{s,fr}$ is calculated using the correlation reported in [8]. Ø denotes the angle of internal friction and its value is taken as 30° [12,25], p_{fr} is the frictional pressure and is evaluated using the model reported in [11].

$$p_{fr}=\begin{cases}0.05\dfrac{(\alpha_s-\alpha_{s,min})^2}{(\alpha_{s,max}-\alpha_s)^5} & \text{for} \quad \alpha_s>\alpha_{s,min}\\ 0 & \text{for} \quad \alpha_s\le\alpha_{s,min}\end{cases} \tag{9}$$

Here, $\alpha_{s,min}$ denotes the frictional packing limit (*FPL*), $\alpha_{s,max}$ is the maximum attainable solids volume fraction or close packing limit (*CPL*).

Second invariant of deviatoric strain rate tensor, I_{2D}, is estimated as follows:

$$I_{2D}=\frac{1}{6}\{(\overline{\overline{D}}_{s11}-\overline{\overline{D}}_{s22})^2+(\overline{\overline{D}}_{s22}-\overline{\overline{D}}_{s33})^2+(\overline{\overline{D}}_{s33}-\overline{\overline{D}}_{s11})^2\}+\overline{\overline{D}}_{s12}^2+\overline{\overline{D}}_{s23}^2+\overline{\overline{D}}_{s31}^2 \tag{10}$$

$$D_{sij}=\left(\frac{\partial\overline{v}_{si}}{\partial x_j}+\frac{\partial\overline{v}_{sj}}{\partial x_i}\right) \tag{11}$$

Gas-solid inter-phase momentum exchange coefficient is calculated as follows:

$$K_{sg}=\begin{cases}\dfrac{3}{4}\dfrac{C_D\alpha_s\alpha_g\rho_g|\overline{v}_s-\overline{v}_g|}{d_s}\alpha_g^{-2.65} & \text{for} \quad \alpha_g>0.8\\ 150\dfrac{\alpha_s^2\mu}{\alpha_g d_s^2}+1.75\dfrac{\alpha_g\rho_s|\overline{v}_s-\overline{v}_g|}{d_s} & \text{for} \quad \alpha_g\le0.8\end{cases} \tag{12}$$

Ergun's equation for pressure drop through fixed bed is determined using Eq. (13) [26].

$$\frac{\Delta p}{L}=150\frac{(1-\alpha_g)^2}{\alpha_g^3}\frac{\mu U}{(\emptyset_s d_s)^2}+1.75\frac{(1-\alpha_g)}{\alpha_g^3}\frac{\rho_g U^2}{\emptyset_s d_s} \tag{13}$$

Relationship among gas velocity, bed voidage and other parameters at minimum fluidization condition reported in Kunii and Levenspiel [26] is given in Eq. (14).

$$\frac{1.75}{\alpha_{g,mf}^3\emptyset_s}\left(\frac{d_s U_{mf}\rho_g}{\mu}\right)^2+\frac{150(1-\alpha_{g,mf})}{\alpha_{g,mf}^3\emptyset_s^2}\left(\frac{d_s U_{mf}\rho_g}{\mu}\right)=\frac{d_s^3\rho_g(\rho_s-\rho_g)g}{\mu^2} \tag{14}$$

Symbols and notations are explained in nomenclature.

2. Summary of Model Validation at Cold and Non-reactive Hot Flow Conditions

A validation study was performed for the cases under cold flow conditions to establish a range of values of *FPL*. Dimensions of computational domains and particle properties corresponding to experi-

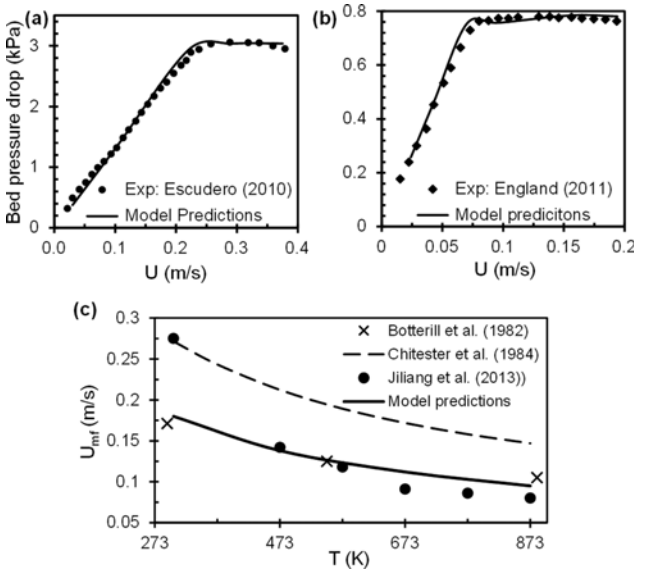

Fig. 1. Comparison of predictions with experimental data for cases corresponding to (a) Escudero [27] (b) England [28] and (c) Jiliang et al. [29].

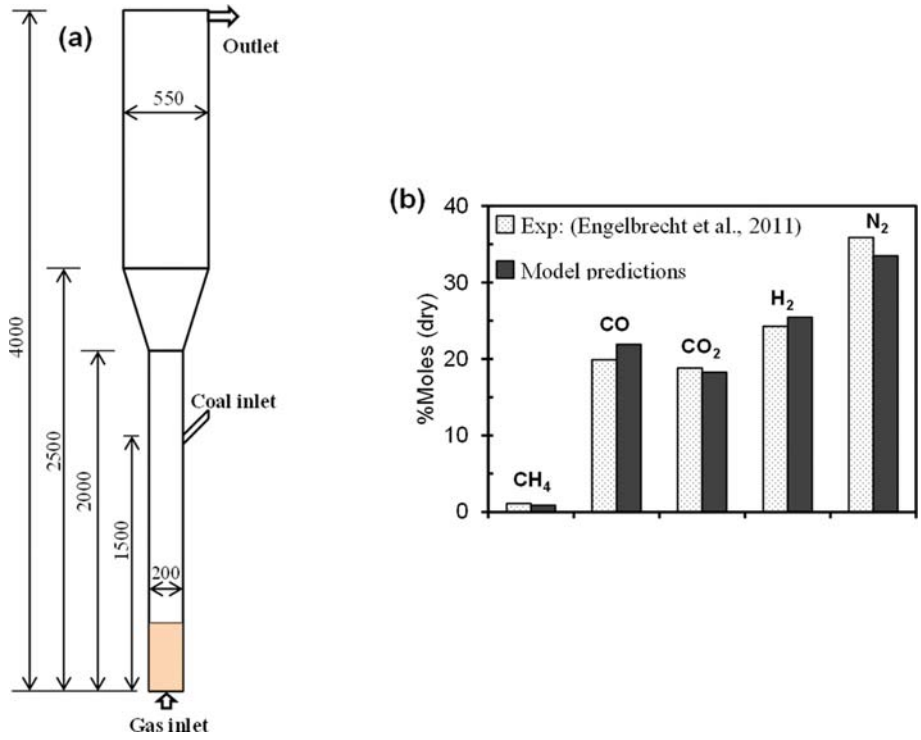

Fig. 2. (a) Computational domain and (b) model validation for reactive flow case.

Table 2. Model parameters used in benchmarking of reactive flow case

Parameters	Values
Computational domain	2D
Total number of cells	7,201
Static bed height	355 mm
Drag model	Huilin-Gidaspow [33]
Particle-particle restitution coefficient	0.9
Specularity coefficient	0.05
Close packing limit	0.6
Frictional packing limit	0.45, 0.5, 0.55 and 0.58
Initial solid volume fraction	0.48
Wall heat loss	5% of total energy input
Volatile cracking scheme	MGAS model [34]
Reaction kinetics	Initial stage: MGAS model [34] Heterogeneous: MGAS model [34] Homogeneous: de Souza-Santos [35]
Time step size (s)	0.0002
Max. iterations/time step	150
Simulation time (s)	125

mental data of [27,28] (cold flow) and [29] (non-reactive hot flow) along with important model parameters are given in Table 1. As shown in Fig. 1, model predictions are in good agreement with reported measurements on bed pressure drop at different superficial gas velocities (cold flow cases) and variation in minimum fluidization velocity with temperature (non-reactive flow at elevated temperatures). Model predictions at elevated temperatures are also compared with the measurements reported in Botterill et al. [30] besides minimum fluidization velocity calculated using Chitester et al. [31] correlation. More details on model validation are reported in [22] and [23] for cold and non-reactive hot flow cases, respectively.

3. Summary of Model Validation for Gas-solid Flows in a Reactive Environment

To benchmark the results of gas-solid flows in reactive environment, the gasifier geometry and operating conditions are taken from the experiments reported in Engelbrecht et al. [32]. Fig. 2 shows the

two-dimensional computational domain. A total of 7201 quadrilateral cells were found to be sufficient as revealed by grid convergence index study reported elsewhere [4]. Important parameters related to model setup are summarized in Table 2. Comprehensive description of the numerical model including governing equations, model parameters pertaining to hydrodynamics and chemical reactions along with model validation is reported elsewhere [4].

RESULTS AND DISCUSSION

1. Effects of *FPL* on Hydrodynamics under Cold Flow Conditions

As reported by Sahu et al. [22], the choices of *FPM* and *FPL* significantly influence the prediction of dense gas-solid flow dynamics, particularly around the incipient fluidization conditions. It was

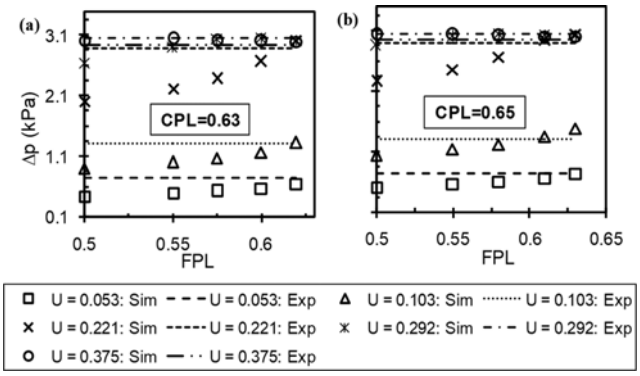

Fig. 3. Effect of *FPL* on prediction of bed pressure drop for two values of *CPL* corresponding to experimental data of Escudero [27] at various superficial gas velocities.

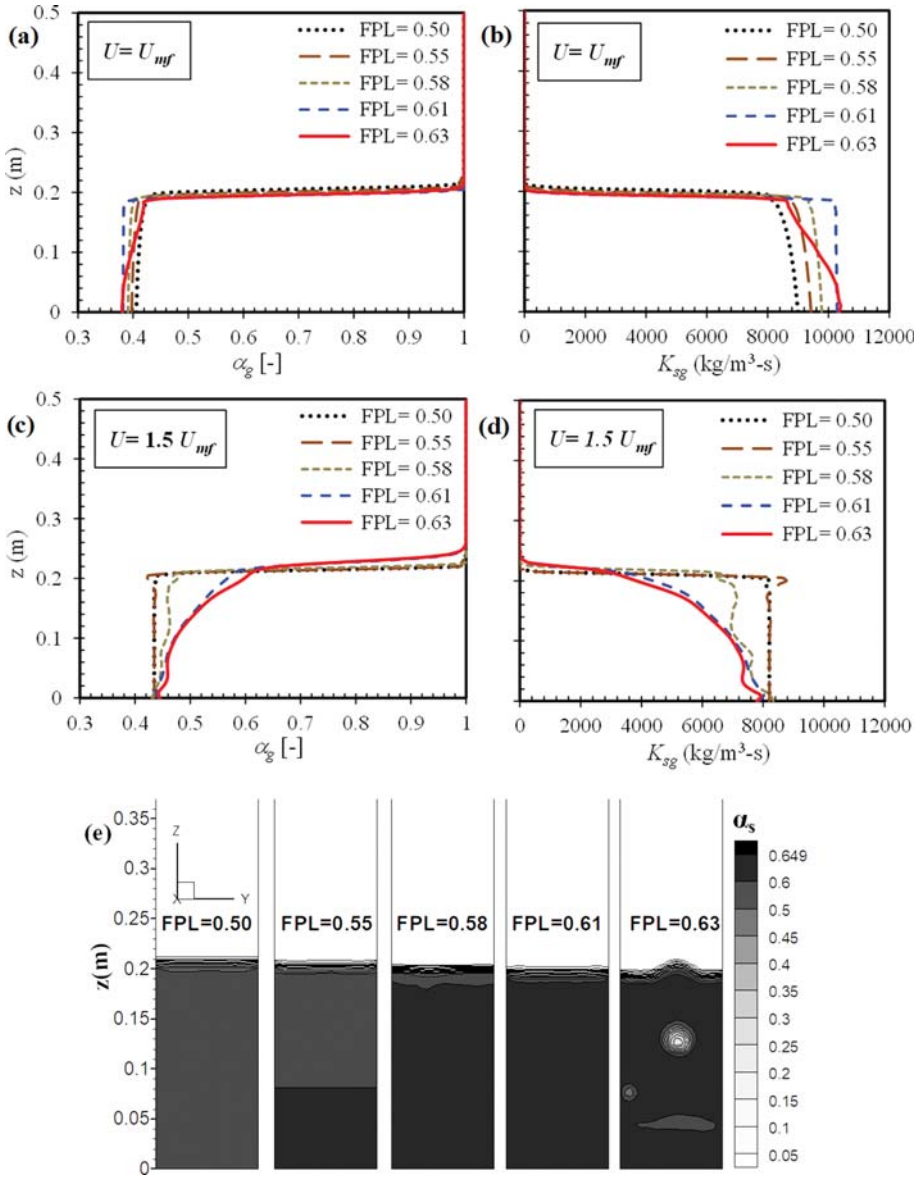

Fig. 4. Variation of time averaged (t=20 s) voidage and K_{sg} along the center line of bed column for different values of *FPL* at ((a), (b)) $U=U_{mf}$ ((c), (d)) $U=1.5U_{mf}$ and (e) contours of instantaneous (t=7.5 s) solids volume fraction at $U=U_{mf}$.

shown that though the effect of *FPM* on hydrodynamics weakens as superficial gas velocity increases beyond U_{mf}, value of *FPL* continues to influence the prediction of pressure drop and flow characteristics.

Fig. 3 presents the effect of frictional packing limit on the prediction of bed pressure drop for two different values of close packing limit (*CPL*), 0.63 and 0.65. Measured pressure drop values at various superficial gas velocities as reported in [27] are also included in the plot. It is noted that the bed pressure drop is under-predicted when value of *FPL* is less than 0.60 (for *CPL*=0.63) and 0.61 (for *CPL*=0.65), particularly when the superficial velocity is less than or equal to the minimum fluidization velocity. It is interesting that the influence of *FPL* on pressure drop prediction increases with an increase in superficial gas velocity and maximum deviation is noticed at U_{mf}. Predicted bed pressure drop is unaffected by the value of *FPL* when superficial gas velocity exceeds the U_{mf}.

Variation of time averaged bed voidage and inter-phase momentum exchange coefficient along the height of the bed at superficial gas velocities equal to U_{mf} (0.221 m/s) and $1.5U_{mf}$ (0.332 m/s) for different values of *FPL* are plotted in Fig. 4. Height is restricted to 0.5 m since the gas volume fraction remains unchanged after around 0.25 m due to absence of particles. It is observed from Fig. 4(a) that voidage in the bed zone increases with a decrease in the value of *FPL* when superficial gas velocity is set to the actual minimum fluidization velocity of 0.221 m/s, except for the largest value of *FPL* examined in this study. For smaller values of *FPL* frictional effects start influencing gas-solid flow dynamics at much lower solids volume fraction besides adding the resulting solids frictional pressure to solids pressure term. Since the solids pressure term accounts for the resistance to particle compaction, a larger effective solids pressure at smaller *FPL* value results in relatively lesser compaction and hence more voidage. Also, larger bed voidage leads to relatively smaller bed pressure drop as evident from Ergun's equation (Eq. (13)). Furthermore, prediction of minimum fluidization velocity is very sensitive to the voidage as noted from Eq. (14). Kunii and Levenspiel [26] reported that voidage at minimum fluidization condition for mono-dispersed particle of a given material and size does not vary much. However, a smaller value of this model parameter (frictional packing limit) is noted to modify the voidage and hence prediction of minimum fluidization velocity. Thus, higher voidage at smaller values of *FPL* leads to over-prediction of minimum fluidization velocity and hence, bubbles may not be present even at $U>U_{mf}$ for group B particles besides delaying the fluidization of bed particles. Quantification of the extent of bias in predicted U_{mf} arising due to use of a particular *FPL* value was not attempted in this study. Profiles of inter-phase momentum exchange coefficient at $U=U_{mf}$ plotted in Fig. 4(b) suggest a reduction in inter-phase momentum exchange and hence drag force by the gas on the particles with decreasing value of *FPL*. Interestingly, voidage profile shows a different trend when *FPL* value is 0.63 at $U=U_{mf}$, particularly, voidage is more in the mid and upper regions of the bed. This indicates the presence of bubbles when *FPL* value is 0.63 as supported by the instantaneous distribution of solids volume fraction depicted in Fig. 4(e). Accordingly, the inter-phase momentum exchange coefficient also shows a decreasing trend in that zone for *FPL*=0.63. Prediction of presence of bubbles at experimentally reported U_{mf} (0.221 m/s) suggests that the minimum fluidization velocity is under-predicted when *FPL* value is 0.63, thus imposing an upper limit on the value of frictional packing limit.

Corresponding profiles of voidage and inter-phase momentum exchange coefficient at $U=1.5U_{mf}$ depicted in Figs. 4(c) and 4(d), respectively, show an opposite trend when compared with the one noticed at $U=U_{mf}$, except for the *FPL* value of 0.63. The reason is that these profiles are plotted along the center line of fluidized bed column in the core region where voidage waves and bubbles formations take place (discussed later) for *FPL* values of 0.58 and higher. Time averaged voidage increases with increase in the value of *FPL* due to formation of bubbles. An increase in bed voidage in core region leads to a reduction in inter-phase momentum exchange coefficient.

Fig. 5 presents the contours of solids volume fraction, frictional pressure and frictional viscosity at $U=1.5U_{mf}$ for different values of *FPL* at a time instant of 20 s. No voidage wave or bubbles are observed for *FPL* values of 0.5 and 0.55, indicating motionless bed particles. For *FPL*=0.58 formation of voidage waves is noticed at various bed heights, even though the bubbles are absent. However,

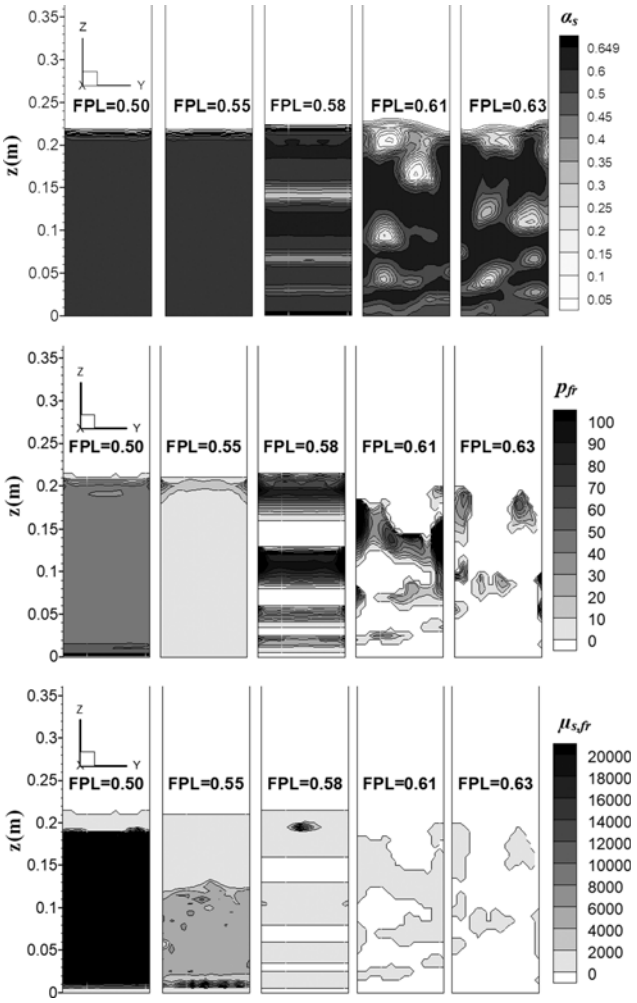

Fig. 5. Distribution of instantaneous (t=20 s) volume fraction (upper row), frictional pressure (middle row) and frictional viscosity (bottom row) of solids phase for different values of *FPL* at $U=1.5U_{mf}$.

bubbles are present throughout the bed when *FPL* is increased to 0.61 and 0.63, predicting a realistic scenario. As the bubbles move upwards, particles surrounding them are also set into motion. Since particles employed in these cases belong to Geldart's group B, bubble formation and hence particle motion is expected as soon as superficial velocity crosses the minimum fluidization velocity. At superficial gas velocity around U_{mf}, the bed particles are in enduring contact, which leads to generation of almost uniform frictional pressure throughout the bed for *FPL* values of 0.5 and 0.55. Early action of frictional pressure results in early resistance to particle compaction and hence somewhat lower solids volume fraction leading to moderate frictional pressures for smaller values of *FPL*. Also, magnitudes of second invariant of deviatoric strain rate tensor of solids phase (I_{2D}) are quite small due to lower values of linear and shear components of strain rate for smaller values of *FPL*. Combination of moderate frictional pressure and lower I_{2D} leads to very high frictional viscosity throughout the bed and hence more energy dissipation for *FPL* values of 0.5 and 0.55. On the other hand, for larger values of *FPL* pockets of higher solids volume fraction near the voidage waves and bubbles are observed. Though, these pockets of high solid volume fraction lead to higher frictional pressures at corresponding discrete locations, frictional viscosity and hence energy dissipation is quite low due to large values of I_{2D} (Fig. 7(a)). Further, relatively higher gas velocity is required to overcome inertia of initially static bed and initiate particle motion for lower values of *FPL*. When gas velocity is close to U_{mf} (=1.5U_{mf}), drag force by the gas on the bed particles is insufficient to overcome the inertia of static bed for lower values of *FPL* (0.5 and 0.55), resulting in static bed regime. For the cases with *FPL* values larger than 0.55, drag force is able to overcome static bed inertia, which subsequently results in formation of voidage waves and bubbles once superficial gas velocity exceeds the U_{mf}.

Distribution of solids volume fraction (upper row), frictional pressure (middle row) and frictional viscosity (bottom row) at U= 1.7U_{mf} for different values of *FPL* are shown in Fig. 6. Corresponding contours of I_{2D} are given in Fig. 7(b). It is observed that the bed particles are motionless for *FPL* value of 0.5; however, unlike at gas velocity of 1.5U_{mf}, bubbles are noticed for *FPL* value of 0.55 at U=1.7U_{mf}. Drag force corresponding to superficial gas velocity of 1.7U_{mf} is able to overcome the static bed inertia with *FPL*=0.55 for this particular case. With further increase in superficial gas velocity the bed is relatively well fluidized and influence of *FPL* on gas-solid flow dynamics reduces. Also, bubble size, its rising motion and total volume occupied by the bubbles increase with an increase in the value of *FPL*.

Contours of time averaged volume fractions of particles for different values of *FPL* at superficial gas velocities of 1.7U_{mf} and 3U_{mf} are presented in Figs. 8(a) and 8(b), respectively. For *FPL* value of 0.5, gas phase is more uniformly distributed within the bed, indi-

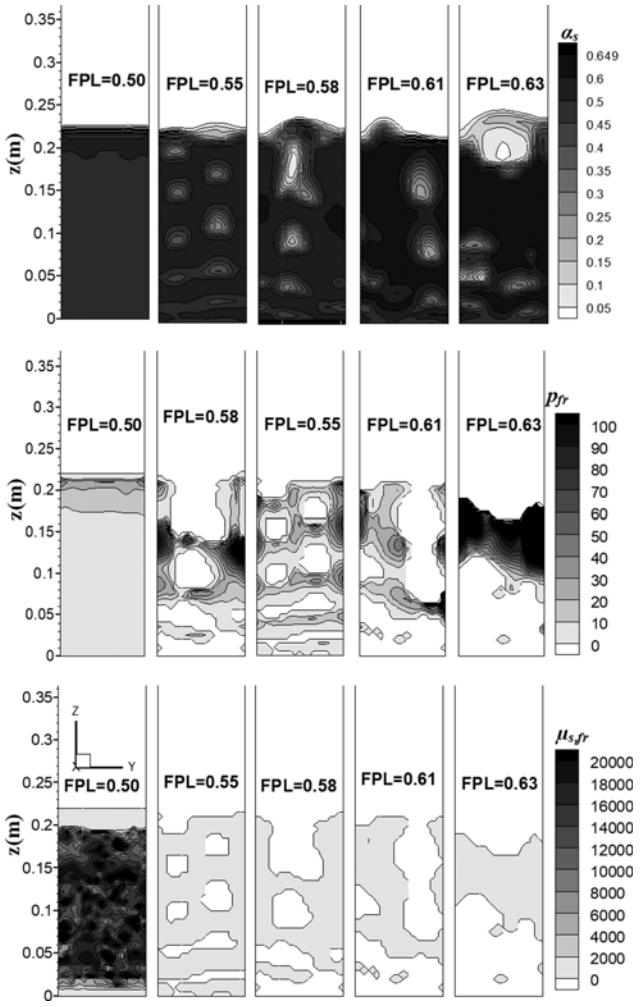

Fig. 6. Distribution of instantaneous (t=20 s) volume fraction (upper row), frictional pressure (middle row) and frictional viscosity (bottom row) of solids phase for different values of *FPL* at U=1.7U_{mf}.

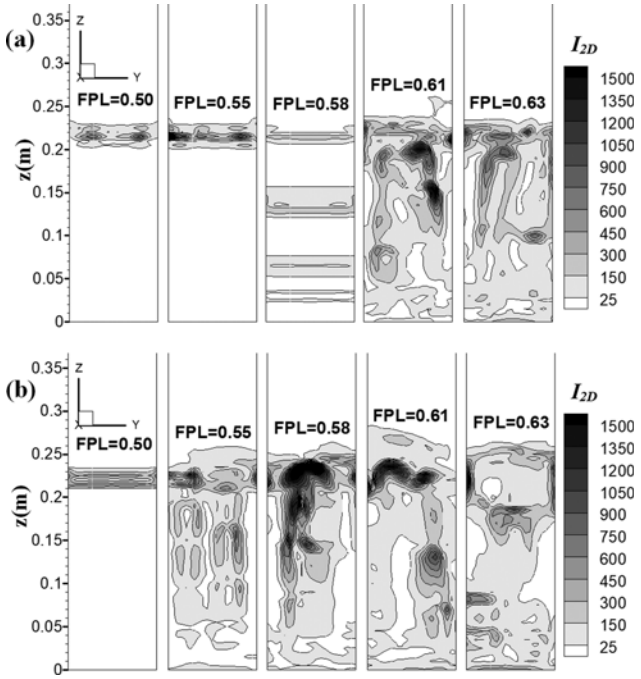

Fig. 7. Contours of instantaneous magnitudes of second invariant of deviatoric strain rate tensor, I_{2D} at (a) U=1.5U_{mf} (b) U= 1.7U_{mf} for different values of *FPL*.

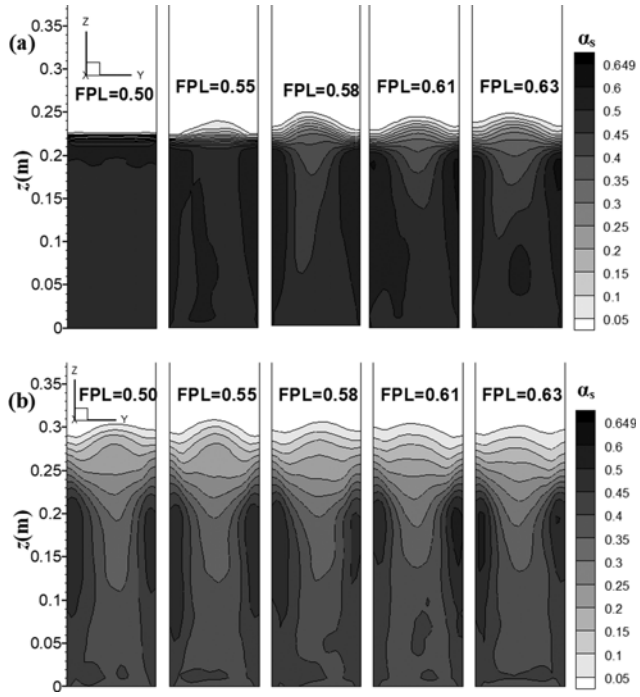

Fig. 8. Effect of *FPL* value on distribution of time averaged solids volume fraction corresponding to Escudero [27] at (a) U= 1.7U_{mf} and (b) U=3U_{mf}.

cating poor particle mixing at 1.7U_{mf}. Thus smaller values of *FPL* may affect the prediction in a reactive flow environment such as solid fuel combustion or gasification. Presence of bubbles helps in better mixing of gas and particles and subsequent enhancement in heat and mass transfer. Therefore it is important for a computational technique to mimic the bubbling behavior as closely as possible, especially in dense gas-solid flows usually encountered in slow bubbling fluidized bed gasifiers. When the superficial gas velocity is further increased to 3U_{mf}, bubbles are observed for all the *FPL* values examined, as evident from Fig. 8(b).

Fig. 9 presents the profiles of time averaged particle velocity and voidage at a height of 0.102 m for different values of *FPL* at superficial gas velocity of 1.5U_{mf}, 1.7U_{mf} and 3U_{mf} corresponding to experimental data of Escudero [27]. At 1.5U_{mf}, particle velocity is zero for *FPL* values of 0.5 and 0.55 and corresponding voidage profiles are also flat throughout the cross-section. As the superficial gas velocity is increased to 1.7U_{mf}, vertical movement of the particles is captured with *FPL* of 0.55; however, particles remain motionless when *FPL* is equal to 0.5. Corresponding voidage profiles confirm the presence of bubbles at all tested values of *FPL* except for 0.5. When superficial gas velocity is equal to 3U_{mf}, particle motion and presence of bubbles are noted for all the tested values of *FPL*. At higher superficial gas velocity, inertia of the static bed is overcome relatively easily besides generating larger velocity gradients and hence larger I_{2D} and lesser frictional dissipation. Thus, with increase in superficial gas velocity the influence of *FPL* on flow characteristics tends to diminish. To further quantity the effects of *FPL* on bubbling behavior and particle velocity model, predictions should be compared with carefully conducted measurements on these flow parameters.

Fig. 10 summarizes the effects of *FPL* on prediction of pressure variation along the height, bed pressure drop and distribution of solids phase volume fraction for the case corresponding to the test data reported in England [28]. Similar to observations made for the cases corresponding to experimental data of Escudero [27], predictions of dense gas-solid flows are better when the *FPL* value is chosen in combination with *CPL* such that the ratio of *FPL* to *CPL* ranges between 0.9 and 0.97. Note that these combinations of *CPL* and *FPL* values are obtained when Johnson et al. [11] frictional pressure model is employed along with Schaeffer's [8] frictional viscosity model.

2. Effects of *FPL* on Hydrodynamics at Elevated Temperature

Variation of bed pressure drop (Δp) predicted by the model as a

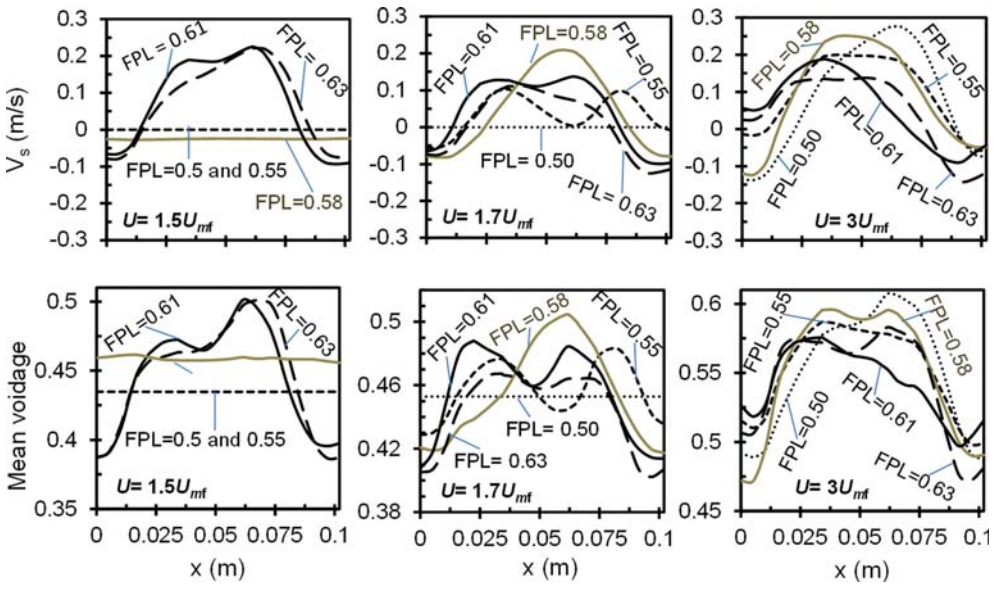

Fig. 9. Effect of *FPL* on particle velocity (top row) and voidage (bottom row) profiles corresponding to Escudero [27].

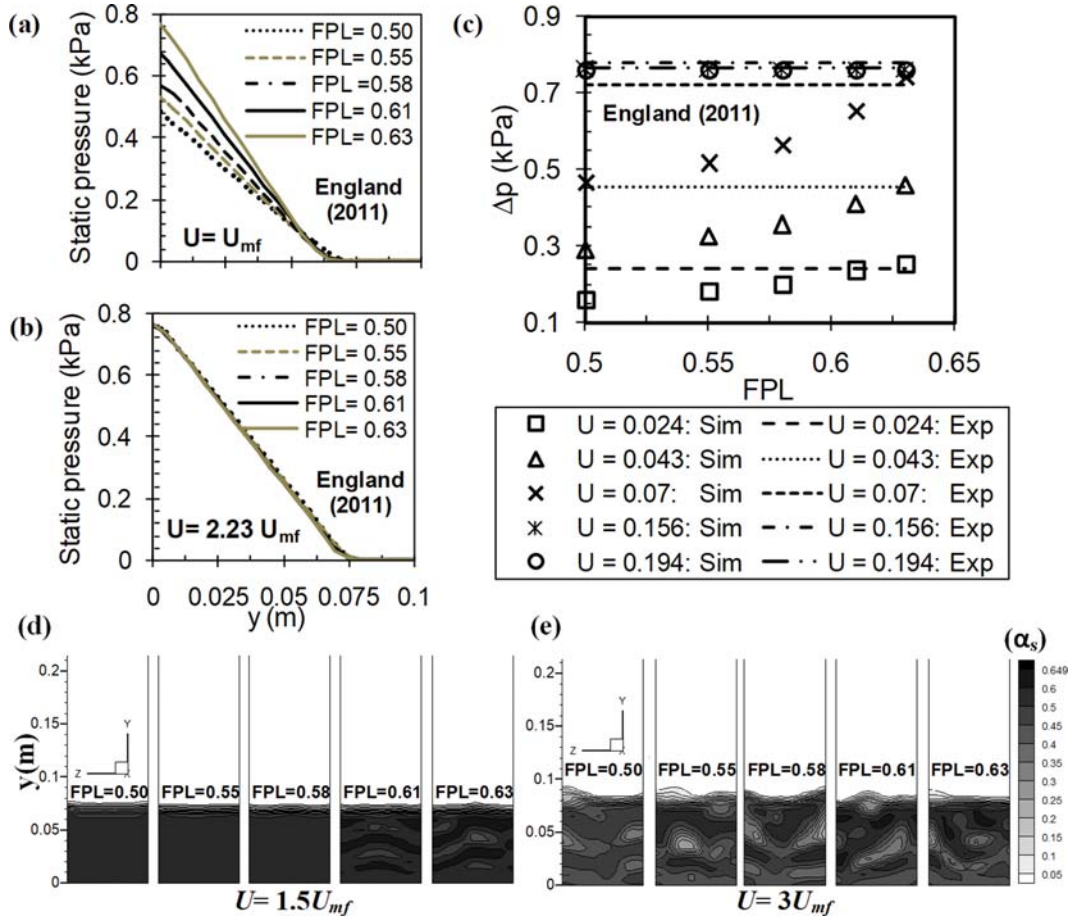

Fig. 10. Effects of *FPL* on (a) variation of static pressure along the height for $U=U_{mf}$ and (b) $U=2.23U_{mf}$ (c) bed pressure and (d) distribution of solids volume fraction at $U=1.5U_{mf}$ and (e) $U=3U_{mf}$ corresponding to experimental values reported in England [28] for different superficial gas velocity.

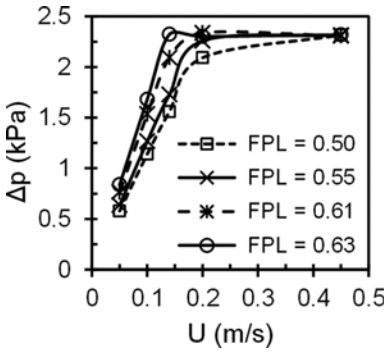

Fig. 11. Effect of *FPL* on prediction of bed pressure drop at 473 K (model set-up as per experimental data reported in Jiliang et al. [29]).

function of superficial gas velocity at an elevated temperature of 473 K is plotted in Fig. 11. It is seen that Δp follows a linearly increasing trend within the minimum fluidization regime for all the tested values of *FPL* and increases with an increase in the value of *FPL*. At a higher gas velocity, Δp is unaffected by the value of *FPL*. It is interesting to note that the predictions obtained using *FPL*= 0.63 match well with the U_{mf} measured experimentally by Jiliang et al. [29]. Influence of *FPL* on gas-solid flow dynamics at an elevated temperature at a superficial gas velocity of 0.213 m/s (well above the U_{mf}) is presented in Fig. 12. The bed particles are at rest for *FPL* values of 0.5 and 0.55, and this observation is further supported by the profiles of time averaged particle velocity and voidage. On the other hand, when the *FPL* value is increased to 0.61 and more, particle motion and bubble movement through the center of the bed are observed. Since bed particles under consideration belong to Geldart's group B, bubble formation and hence particle motion, are expected as soon as superficial gas velocity exceeds the minimum fluidization velocity. Thus, the trends predicted with *FPL* values of 0.61 and 0.63 seem to be more realistic.

3. Effects of *FPL* on Hydrodynamics and Performance of Fluidized Bed Gasifier

This sub-section presents influence of *FPL* on hydrodynamics and performance of bubbling fluidized bed gasifier (BFBG) operating in a reactive ambience. Simulations are performed for different values of *FPL* ranging from 0.45 to 0.58 with a close packing limit of 0.6. In this study, relatively larger sand particles (1.6 mm and 2 mm) are used as bed material to achieve dense gas-solid flow regime, compared to the one employed in experiments (0.65 mm).

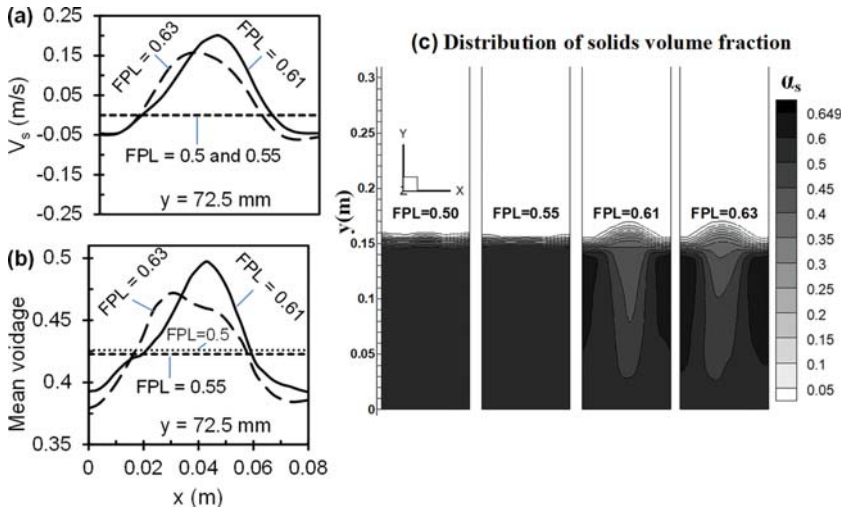

Fig. 12. Effect of *FPL* on (a) particle velocity (b) voidage profile and (c) distribution of particle volume fraction at 473 K for group B particles at U=0.213 m/s.

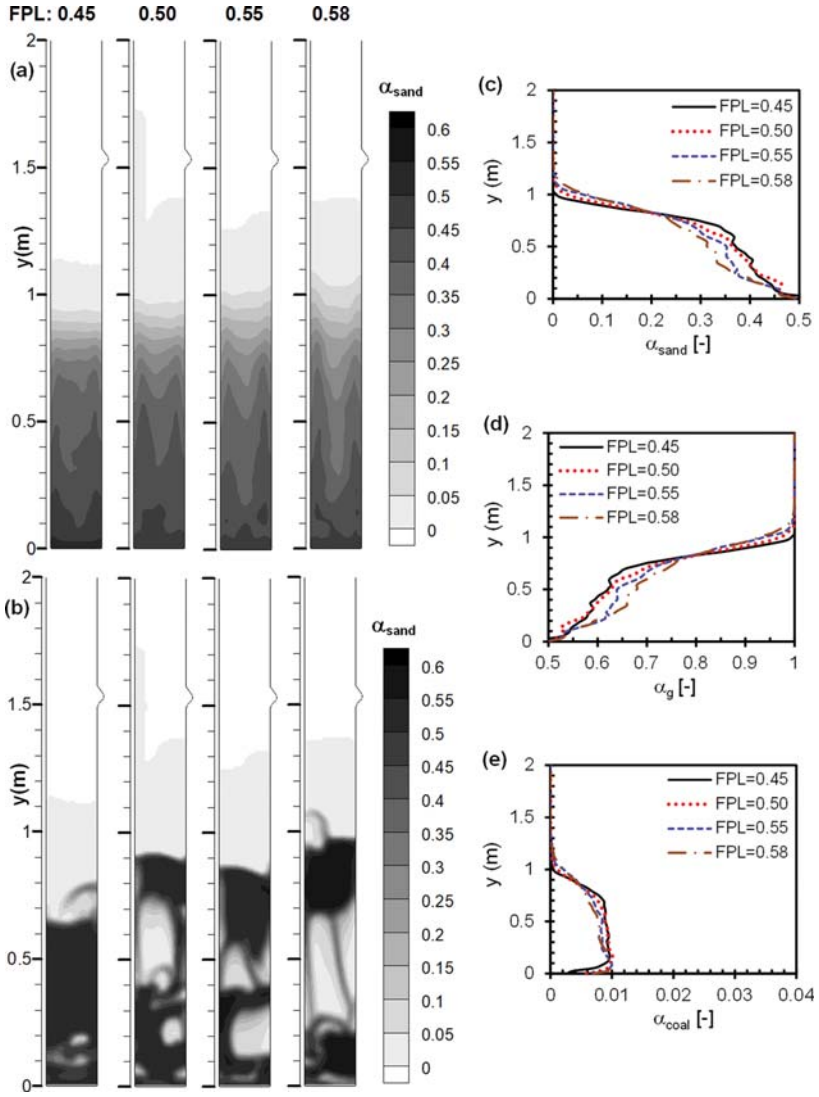

Fig. 13. Contours of (a) time averaged volume fractions of sand (b) instantaneous volume fractions of sand and variations in time averaged volume fractions of (c) sand (d) gas and (e) coal along the height for $d_{s,sand}$=1.6 mm.

Larger of these two particle sizes (d_s=2 mm) is expected to result in slightly denser gas-solid flow regime than with the samller particles (d_s=1.6 mm) for the same gas flow rates. Further, static bed height is kept twice of that used in the experiments to facilitate better flow visualization through the dense regime. All other input data are maintained the same as in Test-2 case of Engelbrecht et al. [32].

3-1. Influence of *FPL* on Reactive Flow Behavior for Small Particles

Fig. 13 shows the contours of time averaged as well as instantaneous volume fractions of sand particles ($d_{s,sand}$=1.6 mm) along with the profiles of time averaged volume fractions of sand, gas and coal for different values of *FPL*. It is observed that time averaged volume fractions of sand, in the core and bottom zones of the gasifier, decrease with an increase in the value of *FPL*. This in turn results in a slight increase in the expanded bed height. Instantaneous dis-

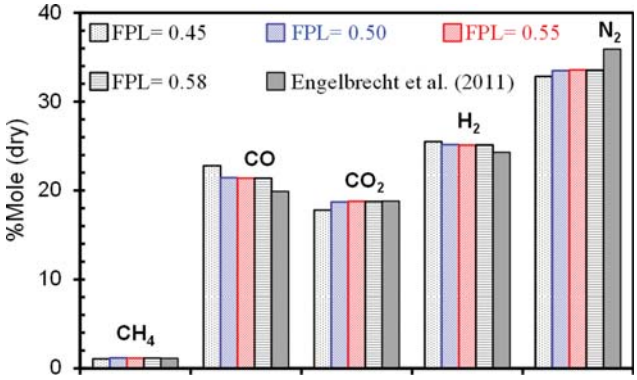

Fig. 14. Comparison of percentage moles of major species in product gas for different values of *FPL* and experimental data of Engelbrecht et al. [32] when $d_{s,sand}$=1.6 mm.

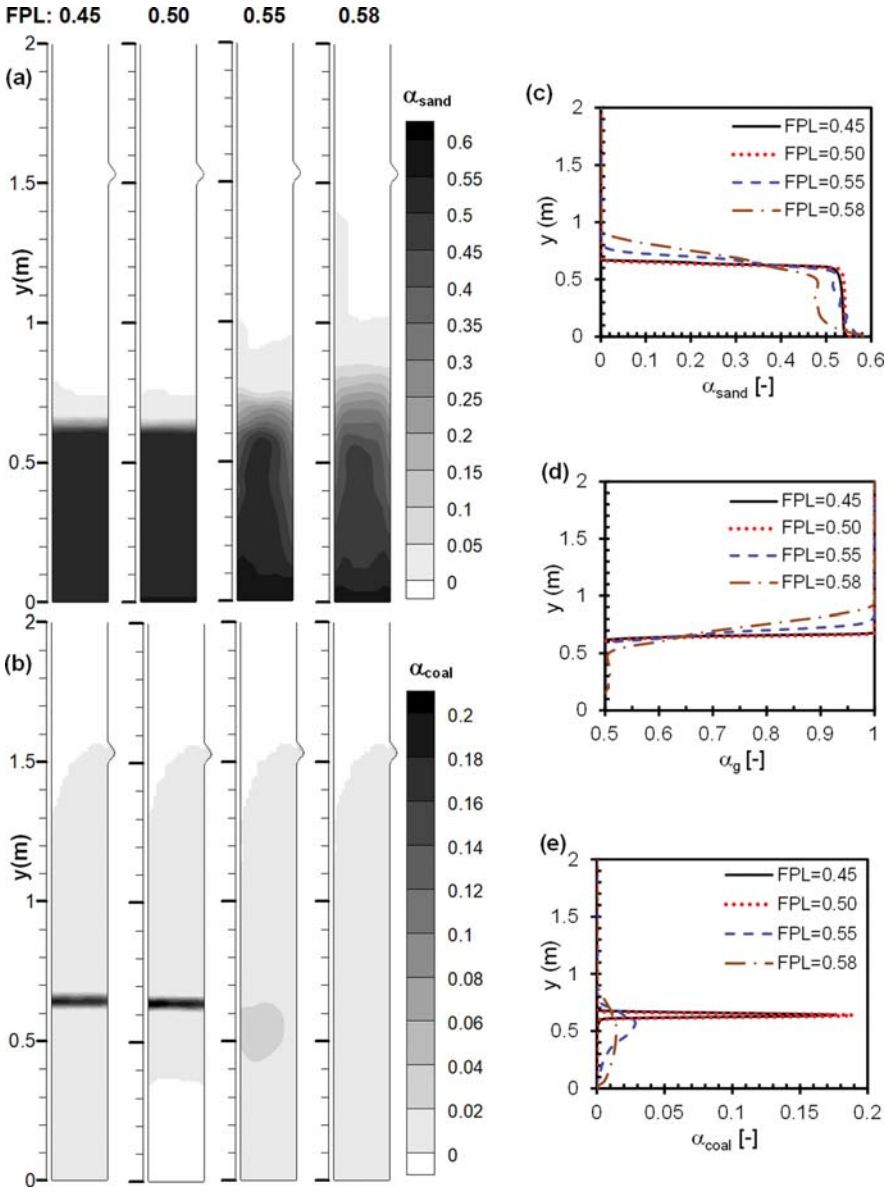

Fig. 15. Contours of time averaged volume fraction of (a) sand and (b) coal and variations of volume fraction of (c) sand (d) gas and (e) coal phases along the height of gasifier when $d_{s,sand}$=2 mm.

tribution of sand volume fractions indicates an increase in bubble size as the value of *FPL* increases. Relatively poor quality of fluidization is evident for *FPL*=0.45. Variations of time averaged volume fractions of different Eulerian phases along the height of the gasifier suggest the tendency of sand particles shifting towards denser region with a decrease in the value of *FPL*. Volume fraction of gas increases in the bed with an increase in the value of *FPL*. On the other hand, distribution of coal is least affected by *FPL* due to its much lower volume fraction than the packing limit.

Comparison of moles of major species in product gas obtained using different values of *FPL* as well as experimental values reported in Engelbrecht et al. [32] is presented in Fig. 14. Mole fractions of various species, determined on a dry basis at the gasifier exit, are time averaged during the last 25 s. Product gas composition is noted to be unaffected by the *FPL* when its value is equal to or greater than 0.5. Also, for *FPL*=0.45, moles of CO and H_2 are more and those of CH_4, CO_2 and N_2 are slightly less.

3-2. Influence of *FPL* on Reactive Flow Behavior for Large Particles

Results presented in sub-section 3.1 suggest that performance of the gasifier is not much altered by the choice of the value of *FPL*, except for *FPL*=0.45, even though the bed hydrodynamics is modified to a noticeable extent. However, as observed for non-reactive flow cases (sub-sections 1 and 2), the effect of *FPL* becomes more pronounced when the bed is denser. Therefore, to further explore the impact of *FPL* on the prediction of hydrodynamics and performance of gasifier, relatively denser gas-solid flow regime is enforced by employing larger sand particles of size 2 mm. Model parameters are kept the same as employed for simulating cases with small particles mentioned in sub-section 3.1. Simulations are executed for 125 s and the data is time averaged during the last 25 s. It is noticed that the number of iterations per time step were significantly more (around 150 iterations as compared to around 30 iterations) to achieve convergence for the cases with *FPL* values of 0.45 and 0.50 than the cases with larger *FPL* values and hence computationally more expensive.

Fig. 15 presents contours of time averaged volume fractions of sand and coal particles, as well as the profiles of volume fractions of sand, gas and coal along the height of the gasifier. Height is restricted to 2 m while plotting the vertical profiles as volume fractions does not change beyond a height of around 1 m. As discussed, the bed of sand particles is almost stationary when *FPL* is 0.45 or 0.5. However, with larger values of *FPL*, frictional stresses in solids are less dominant and hence impart lesser resistance to relative motion between particles. This subsequently results in relatively free movement of particles and subsequent formation of bubbles and bed expansion. Further, the expanded height of the sand bed increases with an increment in *FPL*, and as a result, the zone of higher solid volume fraction tends to diminish. This observation is also supported by Fig. 15(c). Coal particles tend to accumulate above the stationary sand bed for *FPL* values of 0.45 and 0.5, as noticed in Fig. 15(b). The fact that loading of coal particles is less, their volume fraction never exceeds the frictional packing limit. Thus, the frictional stresses are not present in the bed of coal particles; however, their dynamics is influenced by the primary bed (sand) particles. Furthermore, coal particles are not able to penetrate and reach the bottom of the bed for lower *FPL* values, as evident from Fig. 15(e). With an increment in the value of *FPL* mixing of coal and sand particles improves. This results in the penetration of coal particles to the bottom of the bed and their subsequent conversion. Variation of mean volume fraction of gas, depicted in Fig. 15(d), indicates a relatively higher voidage, and hence a better mixing in the bed zone for *FPL* value of 0.58.

Fig. 16 shows the vectors of time averaged velocity of sand and coal particles for different values of *FPL*. Corroborating with the observations made in the beginning of sub-section 3.2, magnitudes

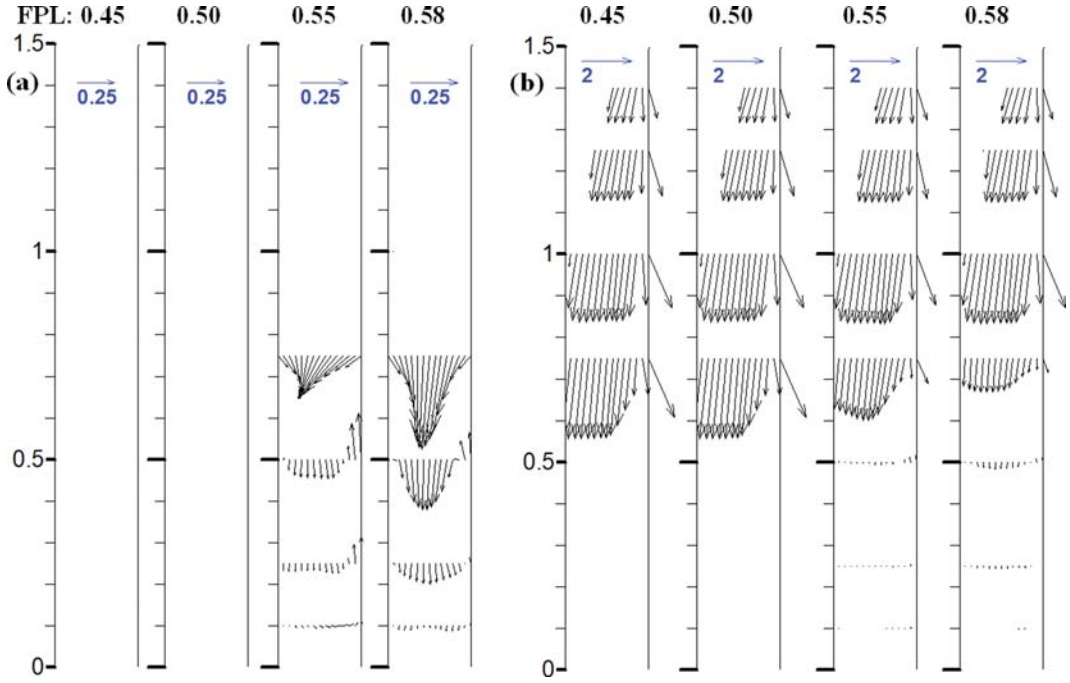

Fig. 16. Vectors of time averaged velocity of (a) sand and (b) coal particles for different values of *FPL* when $d_{s,sand}$=2 mm.

of the velocities of the sand and coal particles in the bed zone are around zero for *FPL*≤0.5. Coal particles fall down at a significantly high velocity from coal inlet to the upper portion of sand bed. For *FPL* values of 0.55 and higher, sand and coal particles are predominantly moving down and the downward motion tends to intensify in the bed zone as the value of *FPL* increases. Downward velocity of coal particles shows a decreasing trend with an increment in the value of *FPL* as increase in the expanded bed height causes reduction in the length between coal inlet and bed upper surface. Also, velocity of sand particles is zero at a reactor height of 1 m and above due to their absence in that region. Thus, gas-solid mixture operates in fixed bed regime when *FPL*≤0.50. For larger values of *FPL*, the sand bed gets loosened paving way for coal particles to penetrate and mix with the sand bed. The extent of mixing of sand and coal particles is enhanced for *FPL*≥0.55.

Distribution of time averaged mass fractions of key species in the gas mixture for different values of *FPL* is presented in Fig. 17, where it is observed that coal particles accumulate at the top of the stationary sand bed forming a thick layer of high volume fraction for *FPL*≤0.50. Due to absence of fuel particles within the sand bed, only reactant gas species such as N_2, O_2 and H_2O are present. As soon as O_2 reaches the surface of the sand bed, it oxidizes the accumulated coal particles to form CO while releasing good amount of heat. A part of CO is further oxidized to CO_2, generating more

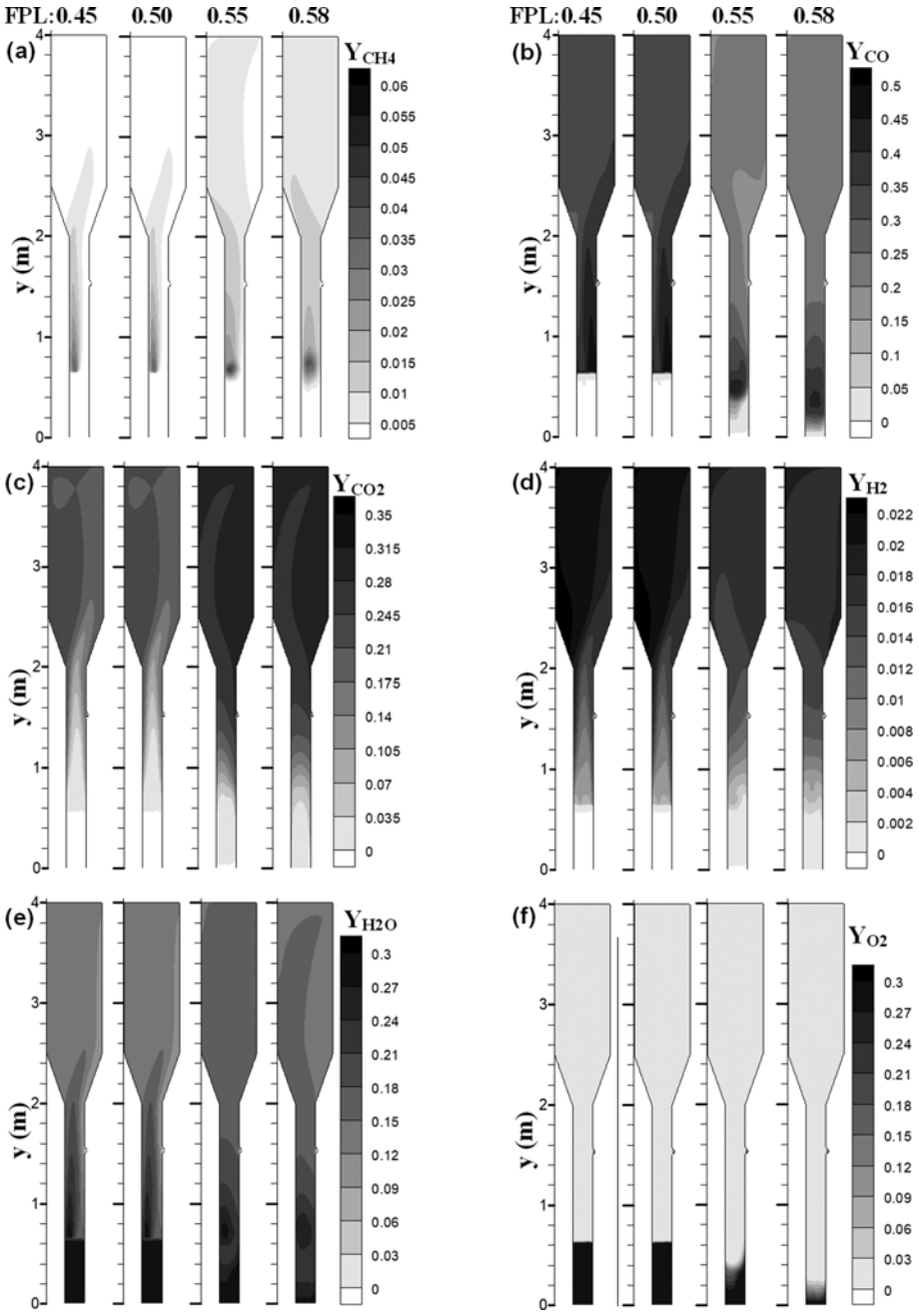

Fig. 17. Distribution of time averaged mass fraction of various species in gas mixture for different values of *FPL* when $d_{s,sand}$=2 mm.

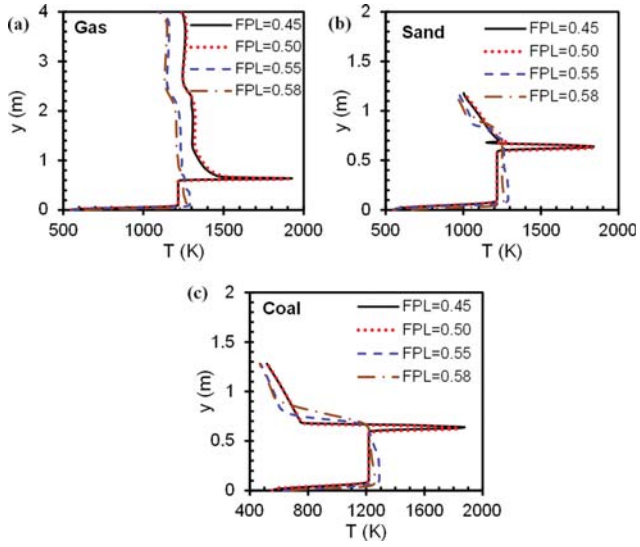

Fig. 18. Time averaged variation of temperatures of (a) gas (b) sand and (c) coal along the height of gasifier when $d_{s,sand}$=2 mm.

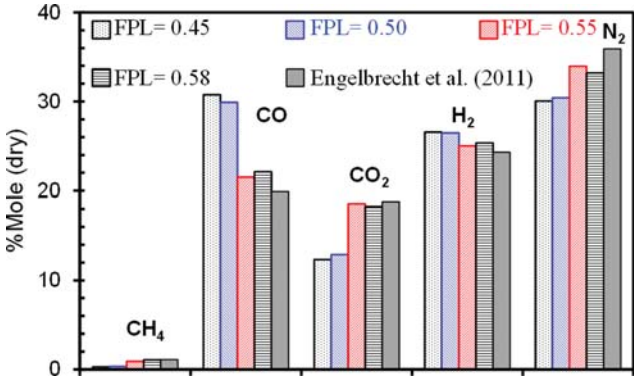

Fig. 19. Comparison of percentage moles of major species in product gas for different values of *FPL* and experimental data of Engelbrecht et al. [32] when $d_{s,sand}$=2 mm.

heat and hence very high temperature in that zone. The CO_2 reacts quickly with high temperature char particles and produces more CO through endothermic Boudouard reaction. Thus, the net mass fraction of CO in the freeboard region and in the product gas is greater when *FPL*≤0.50. On the other hand, the net mass fraction of CO_2 is less for smaller values of *FPL*. Similarly, due to the presence of high temperature zone in the coal bed, steam in reactant gas reacts quickly with hot char for the cases with *FPL*≤ 0.50. Thus, the rapid endothermic steam gasification reaction produces relatively larger amounts of CO and H_2. Presence of high temperature zone and availability of relatively larger amount of oxygen near the sand bed surface for smaller values of *FPL* results in slightly higher consumption of CH_4. Hence, time averaged mass fraction of CH_4 is noted to increase gradually with an increment in the value of *FPL*.

Temperature profiles of gas, sand and coal particles along the height of the gasifier are plotted in Fig. 18. Within the sand bed, temperature is almost constant and relatively less for smaller values of *FPL*. The temperature increases abruptly near the bed surface due to heat release during char oxidation reaction. On the other hand, the rise in temperature is relatively gradual for larger values of *FPL*. Also, in the freeboard region the gas temperature is greater for smaller values of *FPL*. Temperature profiles of sand and coal particles are not plotted in the freeboard zone due to their absence in that region.

Fig. 19 presents the comparison of time averaged mole percentages of important species in the product gas, taken at the gasifier exit, for different values of *FPL*. Experimentally measured values of species mole fractions corresponding to Test-2 of [32] are also plotted. Mole fractions of CO and H_2 are noted to be significantly higher, whereas, that of CO_2 quite less for *FPL*≤0.50. The mole fraction of CH_4 is slightly smaller at lower *FPL* value. Interestingly, the mole fraction of N_2 in the product gas is lesser when *FPL*≤0.50. Fluidizing gas, moisture release, devolatilization and char heterogeneous reactions are the sources of gaseous species in the reactor, and for a given set of operating conditions the quantity of gas released mainly depends on the extent of char conversion. Thus, the lower mole fraction of N_2 in the product gas suggests relatively faster rate of char consumption. The reason for this behavior is the rapid rate of exothermic char oxidation at the bed surface, which results in a very high temperature in the narrow zone. At such high temperatures, rates of steam and CO_2 gasification reactions are also faster, which results in relatively higher rate of char consumption for smaller values of *FPL*.

SUMMARY AND CONCLUSIONS

Sensitivity of the value of frictional packing limit (*FPL*) towards prediction of hydrodynamics of dense gas-solid flows in a non-reactive as well as reactive environment is reported. Several values of *FPL* are used to examine its effects on product gas composition besides evaluating various hydrodynamics features under rigorous as well as slow bubbling conditions. Influence of *FPL* on prediction of bed hydrodynamics and product gas composition revealed that temperature field and product gas species distributions are almost unaffected by *FPL* despite modification in bed hydrodynamics in case of well fluidized bubbling bed. On the other hand, in case of dense gas-solid flows, such as in a slow bubbling fluidized bed gasifier, hydrodynamics as well as temperature and product gas distribution are significantly affected by the value of *FPL*. In case of slow bubbling fluidized bed gasifier, for *FPL*≤0.50, drag force by the gas on the particles could not overcome the static bed inertia due to significantly higher frictional dissipation. This subsequently led to poor mixing of fuel particles with the bed material. Key outcomes of this study are as follows:

• *FPL* affects bed pressure drop prediction only up to $U=U_{mf}$; however, flow characteristics such as particle velocity, particle distribution, bubbling behavior and expanded bed height are influenced by *FPL* in dense regime even when $U>U_{mf}$.

• Ratio of frictional packing limit to close packing limit between 0.9 and 0.97 was found to give better predictions at cold flow conditions.

• *FPL* has similar effect on bed hydrodynamics at elevated temperature (non-reactive) as observed for cold flow conditions.

• Distribution of gas temperature and mole fractions of gas mixture species are almost unaffected by the choice of *FPL* for adequately fluidized bubbling bed gasifier despite modification in the bed dynamics.

• Hydrodynamics and gasifier performance parameters such as volume fraction, velocity, temperature, reaction zone location and product gas composition are considerably affected by choice of the value of *FPL* for slow bubbling fluidized beds.

ACKNOWLEDGEMENT

Authors gratefully acknowledge the computational facility provided by P.G. Senapathy Centre for Computing Resources and National Centre for Combustion Research and Development at Indian Institute of Technology Madras, India.

CONFLICT OF INTEREST STATEMENT

The authors have no conflict of interest to declare.

NOMENCLATURE

C_D : standard drag coefficient
d_s : particle diameter [m]
e_{ss} : particle-particle restitution coefficient
$\overline{g}$: gravity vector [m/s^2]
g_0 : radial distribution function
K_{sg} : interphase momentum exchange coefficient [kg/m^3-s]
L : length or height of the fixed bed [m]
p_{fr} : frictional pressure [Pa]
p_s : solids pressure [Pa]
S_s : source term
t : time [s]
$\overline{v}_g$: gas velocity vector [m/s]
$\overline{v}_s$: solids phase velocity vector [m/s]
α_g : volume fraction of gas or voidage
$\alpha_{g,mf}$: bed voidage at minimum fluidization conditions
α_s : volume fraction of solids phase
$\alpha_{s,max}$: maximum value of solids volume fraction or close packing limit
$\alpha_{s,min}$: threshold value of solids volume fraction at which frictional stress become significant
θ_s : granular temperature [m^2/s^2]
λ_s : solids bulk viscosity [kg/m-s]
μ_s : solids viscosity [kg/m-s]
$\mu_{s,col}$: collisional part of solids viscosity [kg/m-s]
$\mu_{s,fr}$: frictional part of solids viscosity [kg/m-s]
$\mu_{s,kin}$: kinetic part of solids viscosity [kg/m-s]
ρ_s : density of the solids phase [kg/m^3]
$\overline{\overline{\tau}}_s$: particle phase stress tensor [N/m^2]
Ø : angle of internal friction
$Ø_s$: particle sphericity
CPL : close packing limit
FPL : frictional packing limit
FPM : frictional pressure model
KTGF : kinetic theory of granular flows
MGAS : METC gasifier advanced simulation

REFERENCES

1. S. P. Shi, S. E. Zitney, M. Shahnam, M. Syamlal and W. A. Rogers, *J. Energy Inst.*, **79**, 217 (2006).
2. C. Hu, K. Luo, S. Wang, L. Sun and J. Fan, *Chem. Eng. Sci.*, **195**, 693 (2019).
3. M. Mehrabadi, E. Murphy and S. Subramaniam, *Chem. Eng. Sci.*, **152**, 199 (2016).
4. A. K. Sahu, V. Raghavan and B. V. S. S. S. Prasad, *Adv. Powder Technol.*, **30**, 3050 (2019).
5. J. Musser and J. Carney, *Theoretical review of the MFIX fluid and two-fluid models*, DOE/NETL-2020/2100; NETL Technical Report Series; U.S. Department of Energy, National Energy Technology Laboratory: Morgantown, WV (2020).
6. P. Jop, Y. Forterre and O. Pouliquen, *Nature*, **441**, 727 (2006).
7. M. Ferzaneh, A. E. Almstedt, F. Johnsson, D. Pallares and S. Sasic, *Powder Technol.*, **270**, 68 (2015).
8. D. G. Schaeffer, *J. Differential Equations*, **66**, 19 (1987).
9. A. Srivastava and S. Sundaresan, *Powder Technol.*, **129**, 72 (2003).
10. P. C. Johnson and R. Jackson, *J. Fluid Mech.*, **176**, 67 (1987).
11. P. C. Johnson, P. Nott and R. Jackson, *J. Fluid Mech.*, **210**, 501 (1990).
12. L. M. Armstrong, PhD Thesis, Faculty of Engineering and the Environment School of Engineering Sciences, University of Southampton (2011).
13. M. Syamlal, W. Rogers and T. J. O'Brien, MFIX documentation: Theory guide, *National technical information service*, Springfield, VA, DOE/METC-9411004, NTIS/DE9400087, Vol. 1 (1993).
14. G. I. Tardos, *Powder Technol.*, **92**, 61 (1997).
15. Y. T. Makkawi, P. C. Wright and R. Ocone, *Powder Technol.*, **163**, 69 (2006).
16. S. Benyahia, *Ind. Eng. Chem. Res.*, **47**, 8926 (2008).
17. L. M. Armstrong, S. Gu and K. H. Luo, *Chem. Eng. J.*, **168**, 848 (2011).
18. W. Shuyan, L. Xiang, L. Huilin, Y. Long, S. Dan, H. Yurong and D. Yonglong, *Powder Technol.*, **196**, 184 (2009).
19. A. Passalacqua and L. Marmo, *Chem. Eng. Sci.*, **160**, 2795 (2009).
20. S. H. Hosseini, G. Ahmadi, B. S. Razavi and W. Zhong, *Energy Fuels*, **24**, 6086 (2010).
21. M. R. Rahimi, N. Azizi, S. H. Hosseini and G. Ahmadi, *Korean J. Chem. Eng.*, **30**, 761 (2013).
22. A. K. Sahu, V. Raghavan and B. V. S. S. S. Prasad, *Prog. Comput. Fluid Dy.*, **17**, 180 (2017).
23. A. K. Sahu, V. Raghavan and B. V. S. S. S. Prasad, *Int. J. Therm. Sci.*, **124**, 387 (2018).
24. C. K. K. Lun, S. B. Savage, D. J. Jefferey and N. Chepurniy, *J. Fluid Mech.*, **140**, 223 (1984).
25. T. Mckeen and T. Pugsley, *Powder Technol.*, **129**, 139 (2003).
26. D. Kunii and O. Levenspiel, *Fluidization engineering*, 2nd Ed., Butterworth-Heinemann, U.S.A. (1991).
27. D. Escudero, MSc. Thesis, Department of Mechanical Engineering, Iowa State University, Ames, IA (2010).
28. J. A. England, M. S. Thesis, Virgina Polytechnic Institute and State University, Blacksburg VA, USA (2011).
29. M. Jiliang, C. Xioping and L. Daoyin, *Powder Technol.*, **235**, 271

(2013).
30. J. S. M. Botterill, Y. Teoman and K. R. Yuregir, *Powder Technol.*, **31**, 101 (1982).
31. D. C. Chitester, R. M. Kornosky, L. S. Fan and J. P. Danko, *Chem. Eng. Sci.*, **39**, 253 (1984).
32. A. D. Engelbrecht, B. C. North, B. O. Oboirien, R. C. Everson and H. W. P. J. Neomagus, in: Proc. Industrial Fluidization, South Africa (IFSA 2011), **145** (2011).
33. L. Huilin and D. Gidaspow, *Chem. Eng. Sci.*, **58**, 3777 (2003).
34. M. Syamlal and L. A. Bissett, *National technical information service*, Springfield, DOE/METC-92/4104, DE92 00 1111 (1992).
35. M. L. de Souza-Santos, *Fuel*, **68**, 1507(1989).